IEEE Access
Multidisciplinary | Rapid Review | Open Access Journal

Received 30 March 2023, accepted 9 April 2023, date of publication 11 April 2023, date of current version 19 April 2023.

Digital Object Identifier 10.1109/ACCESS.2023.3266364

RESEARCH ARTICLE

Sea Fall Point Measurement Method Based on Cone Angle Intersection

MINGYANG LI[1,2], YI YU[1], CHENGLONG WANG[1], TAO ZHANG[1], XIN GUO[1], AND XINYU PANG[1,2]

[1]Changchun Institute of Optics, Fine Mechanics and Physics, Chinese Academy of Sciences, Changchun 130033, China
[2]University of Chinese Academy of Sciences, Beijing 100049, China

Corresponding author: Yi Yu (13756006195@139.com)

This work was supported in part by the National Natural Science Foundation of China under Grant 51675506, and in part by the Jilin Province Excellent Young Talent Fund under Grant 20190103015JH.

ABSTRACT The naval gun strikes against the sea need to measure the deviation of the fall point to determine the accuracy and hit probability. In order to improve the accuracy of measuring the fall point position of the naval gun, this paper proposes a maritime fall point measurement method based on cone angle intersection, which does not need to use the axis angle data of the equipment and eliminates the dependence on the equipment's axis angle data when measuring accuracy. Firstly, the photographic measurement method is used to achieve automatic optical intersection of single equipment at different moments, using two observation stations and one cooperative target ship. Then, the image data within 10 km from the measured target are collected using two observation stations. The line of sight directions and angles of the two observation stations are combined to measure the target object and the cooperative target ship at each observation station. The constraint of the approximate equal radius of the Earth ellipsoid is added under close range conditions. The cone angle intersection model mapping relationship is established. Finally, the coordinate position of the target object in three-dimensional space is calculated using field tests at sea and compared with the actual position for analysis. The experimental results show that the measured fall point is within 5 m in the range of 700 m with a ratio of more than 75%. This has increased the range of measurement accuracy processing and proved the feasibility of the measurement method. The method can be used for calibrating large and medium caliber naval gun firing to the sea to improve the firing accuracy of the weapon. It has guiding significance for measuring the fall point position of naval guns at sea.

INDEX TERMS Maritime fall point measurement, cone angle intersection, photographic measurement, optical intersection.

I. INTRODUCTION

The photoelectric theodolite is an instrument that measures the azimuth and elevation angles of a target in real-time and captures its image. The circular grating is installed on the vertical and horizontal axes of the theodolite and is used to measure the axis angle data, i.e., the azimuth and elevation angles of the theodolite. The prerequisite for using the axis angle data from the photoelectric theodolite is that the theodolite must be leveled. On land, the position of a target can be accurately measured. However, on the sea, which is a moving platform, it is impossible to level the theodolite, and the azimuth and elevation angle data obtained by the equipment are subject to significant errors. Therefore, it is of great research significance to explore how to use the photoelectric theodolite to locate the impact point on the sea and increase the observation distance of the target, in order to achieve more accurate measurements of the fall point.

Target localization methods include laser ranging [1], photography [2], sonar [3], [4], [5], and radar [6], [7], [8], [9], [10], [11], [12], [13], etc. The laser ranging method determines the shell fall location using a rangefinder on the

The associate editor coordinating the review of this manuscript and approving it for publication was Cristian Zambelli.

ship, while the photographic method captures images of the shells' trajectory and fall point with a high-speed camera for analysis. The sonar method detects acoustic signals generated when shells fall into water using sonar equipment installed in underwater equipment, enabling determination of the strike position and off-target volume information [14], [15]. This method is suitable for underwater measurements, but high noise levels may affect measurement accuracy. The radar method can detect shells' flight trajectory and landing position and calculate their off-target volume, but the accuracy may be impacted by factors like the angle and distance of radar detection [16].

In contrast, the photographic method can be applied to various environmental conditions and target types, including static and dynamic targets, and more data information can be obtained through image processing techniques, which can provide richer data support for subsequent analysis and evaluation [17], [18], [19]. However, the accuracy of positioning is limited by weather and terrain conditions. The photography method requires sufficient shooting angles in order to localize the target. A system of positioning methods using geodesy [20], [21] allows for precise positioning and measurement of the fall point of naval gun strikes. Geodetic positioning is a measurement method based on the principles of geodesy. It calculates the coordinates of two points on the Earth by measuring information such as the distance and azimuth between them on the Earth's surface, enabling the positioning and measurement of the target. In practical applications, photography and geodetic positioning methods can be used in combination. The photography method can obtain sufficient information by capturing the target image, while the geodetic positioning method can use this information to calculate the coordinates of each point on the image.

In recent years, researchers have conducted extensive research on achieving high-accuracy positioning of targets using optoelectronic devices. Stich [22] proposed using an ellipsoidal model based on the WGS-84 coordinate system for positioning ground targets. However, this method does not take into account elevation information of the target area, resulting in large positioning errors when the terrain is highly undulating. Zhang et al. [23] proposed a direct ground target localization algorithm based on laser ranging equipment. By using the characteristics of the airborne electro-optical reconnaissance platform to lock and track the target, multiple measurements of the same target are taken to obtain the distance information between the target and the carrier aircraft using the laser ranging device. Bai et al. [24] proposed a multi-target localization method based on a digital elevation model. However, all of these methods rely on airborne optoelectronic platforms for land measurement, making it difficult to apply their research to optoelectronic equipment for maritime fall point measurement. Sadeghi et al. [10] used the reflected signal from the target and the direct signal from the satellite to extract a set of dual-base distance measurement data and satellite position information, and proposed a positioning method considering the zero height of the maritime target and the appropriate combination of measurement signals. However, the authors did not describe the measurement experiment process. The measurement of maritime targets has been a challenging problem for high-precision optical measurement due to the presence of measurement platform sway [25]. In the past, in the absence of reference control points, we usually relied on the attitude measurement data of the local reference of the platform for calculation, but with the current technology level, the error brought by the local reference measurement cannot meet the needs of high-precision measurement.

Due to the limitation of the measurement scene and mode, the photographic method cannot directly solve the Euler angles in the external elements of the camera by the longitudinal axis angle encoder. Using multiple control points, the external calibration solves the camera outer square element with poor accuracy, but the number and distribution position of control points in the field of view are limited, and there is no good solution to this problem. Therefore, we propose a high-precision photoelectric latitude and longitude instrument based on cone angle intersection to measure the fall point at sea. By employing the assistance of 2 observation stations, the direction and angle of the line of sight for both the target object and the cooperative target can be determined with greater accuracy. The introduction of elevation information serves to decrease the impact of sea surface undulation, which can cause positioning errors. Utilizing the cone intersection principle, the coordinate position of the target object can then be calculated within three-dimensional space. This method yields improved precision in position measurement and holds promise for evaluating the accuracy of naval gun firing. Furthermore, it can serve as a pivotal basis for any subsequent firing adjustment.

The main contributions of this paper are as follows:

1. This method eliminates the need to set up multiple control points as cooperative targets on cooperative target vessels and uses a single control point as a cooperative target, reducing the pixel error in the images captured by the fall point image observation system.

2. The proposed method uses two observation stations to measure the direction and angle of the line of sight towards a target and a cooperative target, improving the traditional double station intersection method of the photoelectric theodolite. This increases measurement accuracy, enables longer observation distances, and provides more reliable results by considering elevation information.

3. Field experiments on sea target measurement were conducted, and the method proved to measure the fall point better than 5m within a range of 700m, fulfilling the requirements for naval gun system testing. It can be used for calibrating naval guns firing against the sea, improving firing accuracy, and has a guiding significance for measuring the fall point position of naval guns at sea.

The paper is organized as follows: Section II introduces the measurement methods of azimuth and pitch angles of fall points at sea; Section III analyzes the mathematical model of cone angle intersection method with elevation information; Section IV describes the process of field test at sea and analyzes the results of measurement data; Finally, we conclude this paper in Section V.

II. AZIMUTH AND PITCH ANGLE MEASUREMENT METHOD FOR SEA FALL POINT

A. COORDINATE SYSTEM ESTABLISHMENT

A mathematical model is established to measure the geodetic coordinate systems (B, L, H) of one cooperative target ship and two measurement ships using a shipboard satellite positioning system, as detailed in references [26], [27]. The survey ships are denoted as C1 and C2, the cooperative target ship as B3, and the landing point at sea as HB. Phase-difference GPS positioning units are utilized to measure the geocentric geodesic coordinates (B, L, H) of the cooperative target ship and survey ships, which are then converted to the geocentric spatial right-angle coordinate system (X, Y, Z).

The geocentric spatial Cartesian and geocentric geodetic coordinate systems are commonly used for GPS positioning, and their relationships are shown in Figure 1. In the geocentric right-angle coordinate system, the origin O is at the center of the Earth's mass, the Z-axis points towards the North Pole, the X-axis towards the longitude origin E, and the Y-axis is perpendicular to the XOZ plane to form a right-handed coordinate system. Point P's coordinates can be expressed as P(X, Y, Z) in this system. In the geocentric geodetic coordinate system, the center of the Earth's ellipsoid coincides with the Earth's center of mass, and the short axis of the ellipsoid coincides with the rotation axis. The initial geodetic meridian plane coincides with the initial astronomical meridian plane, and point P's coordinates can be expressed as P(B, L, H) in this system.

where L denotes the geodetic longitude, the angle between the geodetic meridian plane passing through point P and the initial geodetic meridian plane; B denotes the geodetic latitude, the angle between the normal direction of point P and the equatorial plane; and H denotes the geodetic height, the distance from point P to the ellipsoidal plane along the normal direction.

The conversion equation of geocentric geodesic coordinates (B, L, H) and geocentric spatial rectangular coordinates (X, Y, Z) under the same reference ellipsoid can be expressed as follows:

$$\begin{bmatrix} X \\ Y \\ Z \end{bmatrix} = \begin{bmatrix} (N+H)\cos B\cos L \\ (N+H)\cos B\sin L \\ (N-Ne^2+H)\sin B \end{bmatrix} \tag{1}$$

$$N = \frac{a}{\sqrt{1-e^2\sin^2 B}} \tag{2}$$

$$e^2 = \frac{a^2-b^2}{a^2} \tag{3}$$

In equation (1), X, Y, Z are the geodetic right-angle coordinates of the experimental vessel, B, L, H are the geocentric coordinates of the experimental vessel, and N is the radius of curvature in the prime vertical. a is the long semi-axis of the Earth's ellipsoid in Equation (2) and Equation (3), a = 6378137 m. b is the short semi-axis of the Earth's ellipsoid in Equation (3), b = 6356752 m. e is the first deviation, e = 1/298.257.

B. ANGLE MEASUREMENT METHOD BASED ON MULTIPLE CONTROL POINTS

The system employs an ultra-high resolution photoelectric theodolite to capture images of a cooperative target ship and sea fall point. It utilizes a dynamic image surface fitting measurement method based on Euclidean spatial affine transformation when more than two measurement reference points are available. This method generates high-precision target fall point measurement data through post-processing, relying on the six-parameter model method. Three cooperative targets are positioned on the ship B3 as control points in the six-parameter model, as illustrated in Figure 2. To account for the cooperative target's rotation and changes in relative position during travel, a multi-surface three-dimensional target is used. The target's bottom plate is dyed black to enhance the imaging signal-to-noise ratio, and a high-brightness LED array is placed at the center of the imaging surface. The position indication module is a 1m square, and the LED array's size is approximately 50cm. If we calculate according to the azimuthal direction, 5k image elements cover a 1km range, and the target can be imaged by approximately

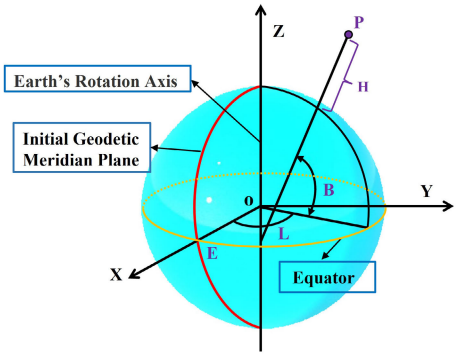

FIGURE 1. Geocentric geodetic coordinate system and geocentric spatial Cartesian coordinate system.

FIGURE 2. Arrangement of cooperation goals.

5×5 image elements. This meets the requirements for imaging and precise positioning without the need to light up the LEDs. In cases of poor weather conditions and visibility, the LED array can be used as a reference mark for illumination.

Set up the control points, establish corresponding equations based on the six-parameter model k_0, k_1, k_2, k_3, k_4 and k_5, solve for the corresponding parameters, and use them to calculate the angle of the fall point at sea. Then, determine the spatial coordinates of the fall point and its deviation from the target ship by intersecting data from the two measurement vessels.

The dynamic image plane fitting six-parameter model based on the Euclidean spatial affine transformation is constructed as follows. As a fundamental transformation in affine geometry, the affine transformation is defined as:

$$C(X) = T(X) + a \tag{4}$$

where T is a non-singular linear transformation, if $a \in R^n$, then the transformation C is called affine transformation.

The theoretical angle of the target and its off-target amount on the imaging target surface are two-dimensional vectors, which can be expressed as their affine transformation on a two-dimensional Euclidean space as:

$$\begin{bmatrix} A \\ E \end{bmatrix} = \begin{bmatrix} k_1 & k_2 \\ k_4 & k_5 \end{bmatrix} \begin{bmatrix} x \\ y \end{bmatrix} + \begin{bmatrix} k_0 \\ k_3 \end{bmatrix} \tag{5}$$

The calculated angle A, E represents the orientation of the cooperative target with respect to the measuring station and can be derived from the GPS positioning unit data of control point coordinates and measuring station coordinates. x, y are the lateral longitudinal off-target quantities imaged by the target on the image plane. k_0, k_3 are the translation vectors, $\begin{bmatrix} k_1 & k_2 \\ k_4 & k_5 \end{bmatrix}$ is the matrix formed after rotation, k_i are real numbers that determine the corresponding transformation relationship between the angle of the target and its off-target amount on the image plane. The corresponding transformation relations can be expressed as follows:

$$\begin{cases} A = k_1 \times x + k_2 \times y + k_0 \\ E = k_4 \times x + k_5 \times y + k_3 \end{cases} \tag{6}$$

According to the three cooperative target control points, six parameters k_0, k_1, k_2, k_3, k_4, and k_5 can be derived, respectively, and their formulas can be expressed as follows:

$$\begin{cases} A_1 = k_1 \times x_1 + k_2 \times y_1 + k_0 \\ A_2 = k_1 \times x_2 + k_2 \times y_2 + k_0 \\ A_3 = k_1 \times x_3 + k_2 \times y_3 + k_0 \end{cases} \tag{7}$$

$$\begin{cases} E_1 = k_4 \times x_1 + k_5 \times y_1 + k_3 \\ E_2 = k_4 \times x_2 + k_5 \times y_2 + k_3 \\ E_3 = k_4 \times x_3 + k_5 \times y_3 + k_3 \end{cases} \tag{8}$$

where (x_1, y_1), (x_2, y_2), (x_3, y_3) are the off-target amounts of their images on the image plane, respectively. (A_1, E_1), (A_2, E_2), (A_3, E_3) are the angles of the three cooperative target control points relative to the measurement station, respectively.

Based on the off-target amount of the falling target and the derived six parameters, the angle of the fall point under the measuring station can be calculated as:

$$\begin{cases} A_{c1} = k_1 \times x + k_2 \times y + k_0 \\ E_{c1} = k_4 \times x + k_5 \times y + k_3 \end{cases} \tag{9}$$

Similarly, the angle (A_{c2}, E_{c2}) of the target in the other measuring station can be found, and the 3D coordinates of the landing target can be obtained by intersection calculation based on the coordinates of the two measuring stations.

Among the 3 cooperative targets of the cooperative target ship, the farthest 2 are only about 20 - 40 pixels apart from each other, which can be represented by Figure 3, while the measured target may be more than 2000 pixels away from the cooperative target ship, which will cause the error of the six-parameter model to be magnified. The green rectangular box is the cooperative target ship, the blue circle is the laid out cooperative target, and the red rectangular box is the measured drop target. 3 cooperative targets are visible in the upper blue circle, 2 cooperative targets are visible in the lower blue circle, and the other one cooperative target is obscured.

Considering the ocean complexity, the focal length of the equipment is short when the target is far away, and the cooperative target imaging is small due to the limitation of the length of the target ship where the cooperative target is deployed. 3 cooperative targets exist adjacent, obscured, or not clearly observed, etc. The 3 cooperative targets observed from the equipment can be almost equivalent to the same one, which cannot effectively distinguish the reference points set by themselves on the cooperative targets, affecting the accuracy of the six-parameter model method based on multiple control points.

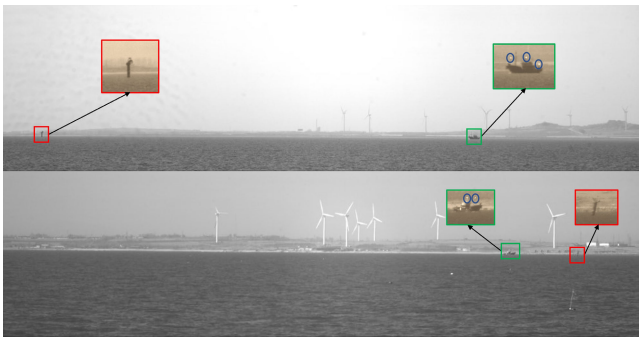

FIGURE 3. Imaging of 3 cooperative targets at sea.

C. ANGLE MEASUREMENT METHOD BASED ON SINGLE CONTROL POINT

Considering the existence of two measurement vessels that can only see one cooperative target at the same time. None of the three cooperative targets set up can be seen, as shown in Figure 4, and we use the angle measurement method based on a single control point.

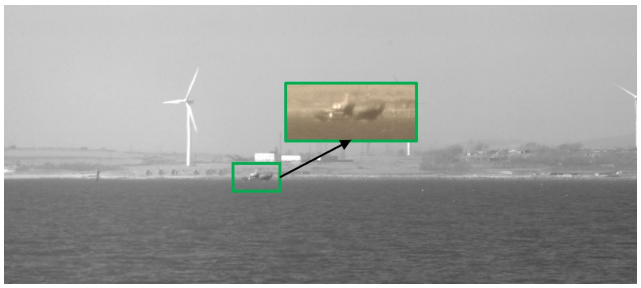

FIGURE 4. Cooperative target ship single imaging.

Suppose the geodesic space right-angle coordinates of survey ship C1, C2, and cooperative target ship B3 are C1(X_1, Y_1, Z_1), C2(X_2, Y_2, Z_2), B3(X_3, Y_3, Z_3), and HB(X, Y, Z). The azimuth and pitch angles of the cooperative target ship B3 for the measurement ships C1, C2 can be expressed as:

$$\begin{cases} A_{C1} = \arctan \dfrac{Z_3 - Z_1}{X_3 - X_1} \\ E_{C1} = \arctan \dfrac{Y_3 - Y_1}{\sqrt{(Z_3 - Z_1)^2 + (X_3 - X_1)^2}} \end{cases} \tag{10}$$

$$\begin{cases} A_{C2} = \arctan \dfrac{Z_3 - Z_2}{X_3 - X_2} \\ E_{C2} = \arctan \dfrac{Y_3 - Y_2}{\sqrt{(Z_3 - Z_2)^2 + (X_3 - X_2)^2}} \end{cases} \tag{11}$$

where A_{c1} and E_{c1} are the azimuth and pitch angles of the cooperative target ship relative to the measuring ship C1, respectively, and A_{c2} and E_{c2} are the azimuth and pitch angles of the cooperative target ship relative to the measuring ship C2.

The images are taken by high-precision photoelectric latitude and longitude instruments of measurement vessels C1 and C2, and the two photoelectric latitude and longitude instruments take images of the measured fall point HB and the cooperative target ship B3 in real time. The first image and the second image containing both the cooperative target ship and the measured fall point are obtained, respectively. During the operation of the high-precision measurement photoelectric latitude and longitude instrument, the servo control subsystem uses calculations and control to point the control point on the cooperative target ship based on the coordinates of the control point, the coordinates of the current station, and other data. The goal is to ensure that the control point is as close to the center of the camera target surface as possible. However, there are situations where the actual imaging of the control point deviates from the center of the target surface, as shown in Figure 5 where point C is not at the same position as point O. The amount by which the target T is off-target relative to the approximate center is denoted by (x_t, y_t). The horizontal and vertical off-target amounts of the measured target relative to the center of the first and second images are calculated based on the pixel points, respectively. In this context, the O point refers to the main point (center) of the target surface of the high-resolution camera, the C point is the actual imaging position of the cooperative target ship control point on the camera target surface, and the T point is the imaging position of the fall point on the camera target surface.

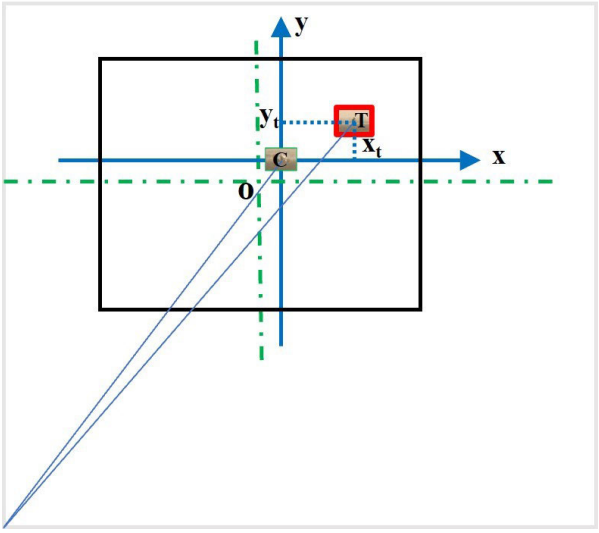

FIGURE 5. Miss distance diagram.

Suppose that the imaging position of the control point of the cooperative target ship on the camera target surface is approximately at the center. The off-target amounts of the imaging fall points of the two measurement ships relative to this approximate center are (x_{t1}, y_{t1}) and (x_{t2}, y_{t2}), respectively. Combining these values with the pitch and azimuth angles of the cooperative target ship for measurement ships C1 and C2, the synthetic angle of the meridian target can be calculated using the conventional method. The formula can be computed as follows:

$$\begin{cases} \alpha_1 = \arctan \dfrac{x_{t1}}{f \cos E_{C1} - y_{t1} \sin E_{C1}} \\ A_1 = A_{C1} + \alpha_1 \\ E_1 = \arctan \dfrac{(y_{t1} \cos E_{C1} + f \sin E_{C1}) \cos \alpha}{f \cos E_{C1} - y_{t1} \sin E_{C1}} \end{cases} \tag{12}$$

$$\begin{cases} \alpha_2 = \arctan \dfrac{x_{t2}}{f \cos E_{C2} - y_{t2} \sin E_{C2}} \\ A_2 = A_{C2} + \alpha_2 \\ E_2 = \arctan \dfrac{(y_{t2} \cos E_{C2} + f \sin E_{C2}) \cos \alpha}{f \cos E_{C2} - y_{t2} \sin E_{C2}} \end{cases} \tag{13}$$

where α_1 and α_2 are alternative process quantities in the calculation, f is the focal length of said first optical system and said second optical system when acquiring images, and (A_1, E_1), (A_2, E_2) are the angles of the measurement vessels C1, C2 corresponding to the fall points.

III. CONE ANGLE INTERSECTION DATA PROCESSING METHOD

A. ANALYSIS OF SEA LEVEL EARTH CURVATURE EFFECTS

Since the Earth is an ellipsoid, the measuring ship is no less than 8 km away from the cooperative target ship, and they have an elevation difference. Point C represents the location

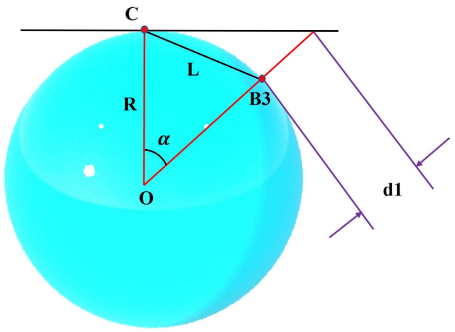

FIGURE 6. Horizontal observation analysis.

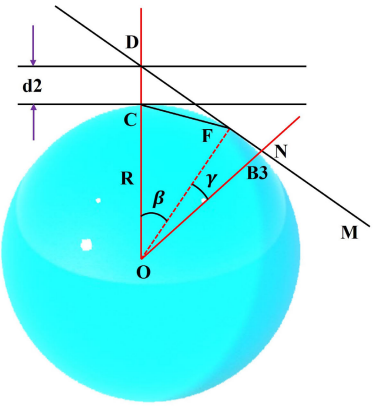

FIGURE 7. Equipment rack height 3m imaging analysis.

of the measuring ship, while point B3 represents the location of the target ship. The distance from point C to B3 is denoted as L, and the radius of the Earth, denoted as R, is 6378137 m, as shown in Figure 6. The angle can be expressed as Equation (14). When the measuring equipment is horizontally pointed at the target ship, there is an elevation difference, d1, relative to point B3 in Figure 6, which can be expressed as Equation (15). Given L = 8 km and R = 6378137 m, we find $\alpha = 0.071865°$ and d1 = 5.017 m. If the equipment is observed horizontally, the target can only be seen 5 m above the level of point B3.

$$\alpha = \arcsin(\frac{L}{R}) \times 2 \tag{14}$$

$$d1 = R \times (\frac{1}{\cos(\alpha)} - 1) \tag{15}$$

According to the work process design and environmental requirements, the equipment is erected at a height of 3 m, assuming that the fall point's height is 4 m during imaging analysis, as shown in Figure 7. Here, d2 = 3 m, which represents the length of CD. A tangent line M is drawn through point D to the Earth's horizontal plane, intersecting it at point F. If the intersection of tangent line M and line OB3 is N, then the length of line B3N is d2. The formula can be expressed as (16) - (18), and the angle is 0.055571°. Given $\alpha = 0.071865°$, we can calculate $\gamma = 0.016294°$ and d2 = 0.25 m. This shows that, during the measurement process, 0.25 m of the 4 m high fall point is obscured by the sea level. Therefore, to achieve complete imaging of the fall point, the equipment needs to be placed at a height of 5 m from the sea level at its location.

$$\beta = \arccos(\frac{R}{R+3}) \tag{16}$$

$$\gamma = \alpha - \beta \tag{17}$$

$$d2 = \frac{R}{cos(\gamma)} - R \tag{18}$$

B. CONE ANGLE INTERSECTION MODEL

Based on the angle measurement method of single control point, we get (A_1, E_1), (A_2, E_2). The angle between measurement vessel C1 and the measured fall point and cooperative target vessel is θ_1, and the angle between measurement vessel C2 and the measured fall point and cooperative target vessel is θ_2, and the formula can be computed as:

$$\begin{cases} \alpha_1 = \arctan \dfrac{x_{t1}}{f\cos E_{C1} - y_{t1}\sin E_{C1}} \\ A_1 = A_{C1} + \alpha_1 \\ E_1 = \arctan \dfrac{(y_{t1}\cos E_{C1} + f\sin E_{C1})\cos\alpha}{f\cos E_{C1} - y_{t1}\sin E_{C1}} \\ \theta_1^2 = A_1^2 + E_1^2 \end{cases} \tag{19}$$

$$\begin{cases} \alpha_2 = \arctan \dfrac{x_{t2}}{f\cos E_{C2} - y_{t2}\sin E_{C2}} \\ A_2 = A_{C2} + \alpha_2 \\ E_2 = \arctan \dfrac{(y_{t2}\cos E_{C2} + f\sin E_{C2})\cos\alpha}{f\cos E_{C2} - y_{t2}\sin E_{C2}} \\ \theta_2^2 = A_2^2 + E_2^2 \end{cases} \tag{20}$$

The 2 survey ships capture the fall point and the position of the cooperating target ship simultaneously. Using 2 high-precision photoelectric theodolite, the target object and the cooperative target ship can be measured in the direction and angle of the line of sight of each shipboard theodolite. The two fields of view intersect, as shown in Figure 8.

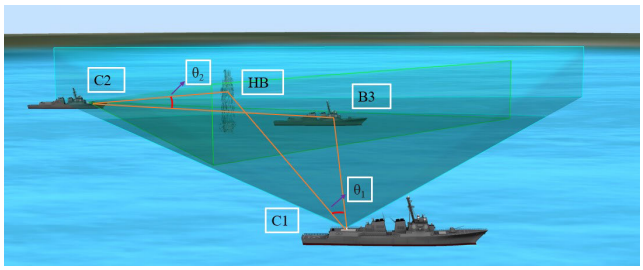

FIGURE 8. Diagram of cone angle intersection measurement.

The cooperative target ship B3 and the fall point target HB are both imaged in the field of view of the two measurement ships, and the two stations target intersection, which can be computed as (21) and (22), shown at the bottom of the next page.

The fall points being measured are on the Earth's surface, as shown in Figure 9. Assuming that the fall point target is

at P1 and the cooperative target ship is at P2, the equatorial circumference of the Earth is about 40,075 km, which is much greater than the sea level target distance. If the test range is within 10 km, then, according to the radius of the sphere being equal, the distance from P1 to point O is equal to the distance from P2 to point O, i.e., OP1 = OP2. The formula can be expressed as:

$$\sqrt{X^2+Y^2+Z^2}=\sqrt{X_3^2+Y_3^2+Z_3^2} \tag{23}$$

If complete imaging of the fall point is required, according to the analysis of the effect of the curvature of the earth at sea level, the equipment needs to be placed at a distance of d1 from the height of the sea level where it is located. Introducing P3, P4, which can be represented by Figure 10, P1, P2, P3 are all points in spherical coordinates, P1, P2 are very close, $OP1 \approx OP2$. P1, P3 are very far away, OP3>OP4, at this time dissatisfied with the equation of soccer coordinates. In order to reduce the error of equation (23), it is necessary to consider the fall point and the elevation of the cooperative target ship. The first and second images, which both contain the cooperative target ship B3 and the measured fall point HB, are combined to obtain the elevation H_{HB} of the measured fall point HB based on the interval of the two specified target points in the vertical direction of the image. The center of the shape of the cooperative target ship B3 and the measured fall point HB imaged in the image are used as the specified target points, with the spherical equation serving as a constraint. The formula can be expressed as:

$$\sqrt{X^2+Y^2+Z^2}=\sqrt{X_3^2+Y_3^2+Z_3^2}-H_{B3}+H_{HB} \tag{24}$$

where H_{B3} is the elevation of the cooperative target ship B3 and H_{HB} is the elevation of the fall point HB.

Using the mathematical model of Eqs. (21), (22), and (24), the traditional way of solving without warp-axis angle encoders, simplifies the photographic back-side intersection measurement model. We used a set of initial solutions to initialize the Newton iteration and then approximated the solution of the system of equations by multiple iterations. In each iteration, we need to solve the system of equations to obtain an approximate solution, and then substitute the approximate solution into the next iteration and continue solving. Eventually, when the number of iterations reaches a certain threshold or the accuracy of the solution reaches a certain requirement, we can stop the iteration and output the final solution. Not simply obtaining the landing point coordinates using the traditional photovoltaic theodolite projection method. To ensure the convergence and accuracy of the algorithm, we also need to control the error during the iterations. The model can derive a series of measurement points that are accurate to the true position of the target at sea.

IV. MEASUREMENT EXPERIMENTS AND RESULTS

We use one cooperative target ship B3 and two measurement ships C1 and C2 loaded with high-precision photoelectric latitude and longitude instruments, as shown in Figure 11, and the measurement ships C1 and C2 carry their own BeiDou receivers and GPS receivers. The lower part is measuring ship C1, the upper part is measuring ship C2, the upper part is due north, the right part is due east, and the cooperative targets are all from west to east. The known position of the hovering target at sea is used to simulate the fall point during the experiment. Measurement ship C1, C2 within 10 km from the measured target, can be imaged in the field of view at the same time. The sailing distance of the cooperative target ship B3 is chosen to be within 1 km of the measured landing point HB, and the cooperative target ship B3 is followed in real time to complete the measurement of the fall point position. Both the cooperative target ship and the survey ship navigate from west to east, i.e., from left to right in the figure. The calibration fitting formula is generated using the outfield calibration data.

Because of the large field of view of the meridian, the digital camera has a lateral resolution of 5120 pixels, which requires aberration correction for different area pixels. When measurement vessel C1 and measurement vessel C2 were within 1 km from the fall point (HB), the longitudinal camera automatically positioned and tracked the cooperative target vessel and the fall point, and the imaging was in the center of the field of view. At the time of the experiment, there was foggy weather on the sea surface, and the images were de-fogged. The acquisition results can be represented in Figure 12. The blue dashed plot represents the video sequence image acquired by measurement vessel C1. The green dashed line represents the video sequence image acquired by measurement vessel C2. Figure 12 (a) shows the image acquired at the previous moment and figure 12 (b) shows the image acquired at the subsequent moment. The two stations are interpreted simultaneously, and the measurement station is equipped with the function of interpreting the current frame while displaying its next image.A_1 and E_1 are the azimuth and pitch angle of the fall point measured by the equipment relative to the measurement vessel C1, and A_2 and E_2 are the azimuth and pitch angle of the fall target measured by the equipment relative to the measurement vessel C2.

$$\cos(\theta_1)=\frac{|(X-X_1)(X_2-X_1)+(Y-Y_1)(Y_2-Y_1)+(Z-Z_1)(Z_2-Z_1)|}{\sqrt{(X-X_1)^2+(Y-Y_1)^2+(Z-Z_1)^2}\sqrt{(X_2-X_1)^2+(Y_2-Y_1)^2+(Z_2-Z_1)^2}} \tag{21}$$

$$\cos(\theta_2)=\frac{|(X-X_2)(X_3-X_2)+(Y-Y_2)(Y_3-Y_2)+(Z-Z_2)(Z_3-Z_2)|}{\sqrt{(X-X_2)^2+(Y-Y_2)^2+(Z-Z_2)^2}\sqrt{(X_3-X_2)^2+(Y_3-Y_2)^2+(Z_3-Z_2)^2}} \tag{22}$$

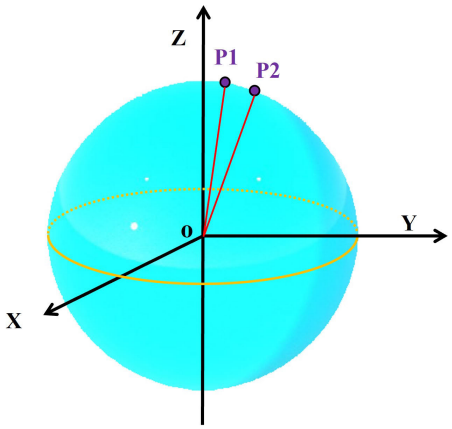

FIGURE 9. Positions of the fall point target and the cooperative target ship.

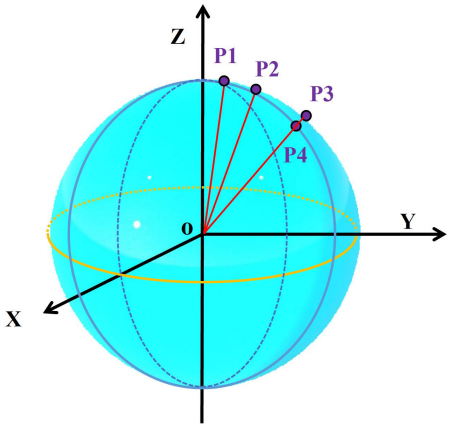

FIGURE 10. Analysis of the elevation of the fall point target and the cooperative target ship.

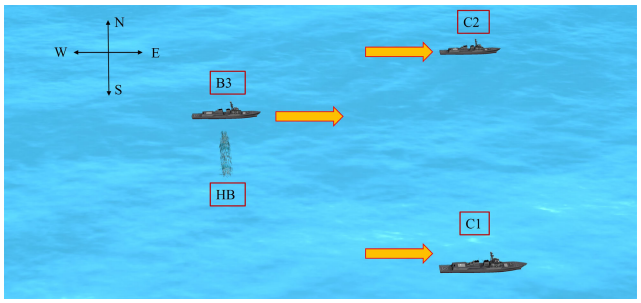

FIGURE 11. Sea-based cooperative target diagram.

The obtained experimental data are processed and the results are analyzed. At the moment of about 300th picture, the direction of A_1 azimuth angle changes, E_1 pitch angle is near 0°, the synthesis angle θ_1 decreases first and then increases. A_2 azimuth angle gradually becomes smaller, E_2 pitch angle fluctuates more strongly in the first period, it can be seen that the measurement ship C2 ship shakes to a greater extent, the synthesis angle θ_2 gradually becomes smaller, which can be expressed in Figure 13.

The experiment verified the rationality of the design idea, measured the data needed for the mathematical model, and

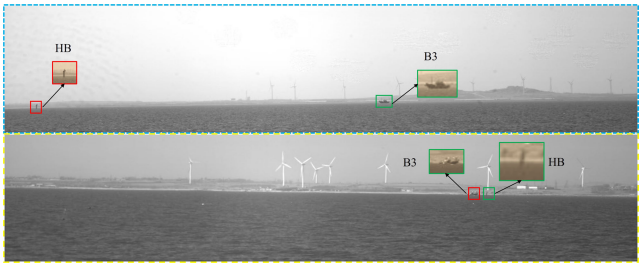

(a) The image acquired at the previous moment.

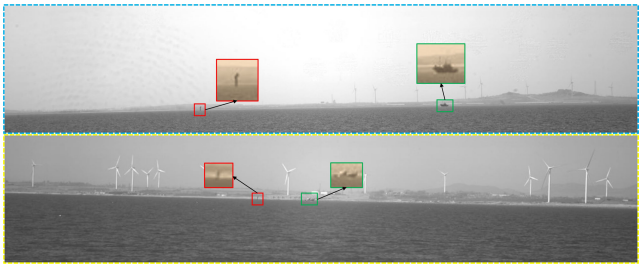

(b) The image acquired at the subsequent moment.

FIGURE 12. Image interpretation of two survey vessels.

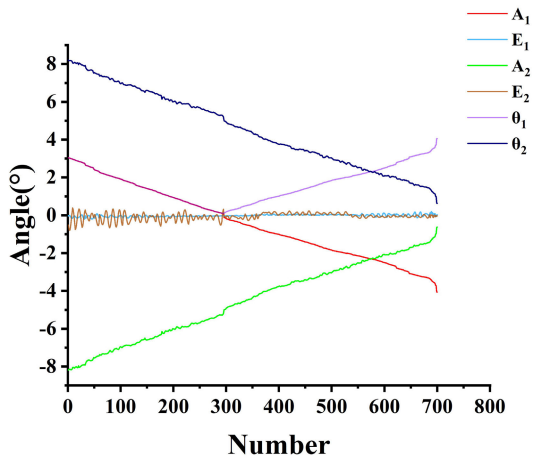

FIGURE 13. The variation of six measurement angles.

TABLE 1. Measurement accuracy ratio.

Distance(m)	Number	Mean Squared Error	Scale better than 5m(%)
700-625	59	1.1629	93.22
625-500	174	1.4571	82.76
450-300	129	1.2565	75.97
300-200	175	0.9963	76.57
200-300	163	0.6897	79.14

obtained the geocentric spatial right-angle coordinates of the measurement vessel C1, C2 and the cooperative target ship. The image data were processed when the cooperative target ship B3 was within 700 meters from the measured fall point. The distance from the cooperative target ship to the fall point is from far to near, starting from 700m until approaching the position of the fall point, and finally sailing away. Using five sets of data analysis, the projection and three-dimensional coordinates of the three planes of the fall

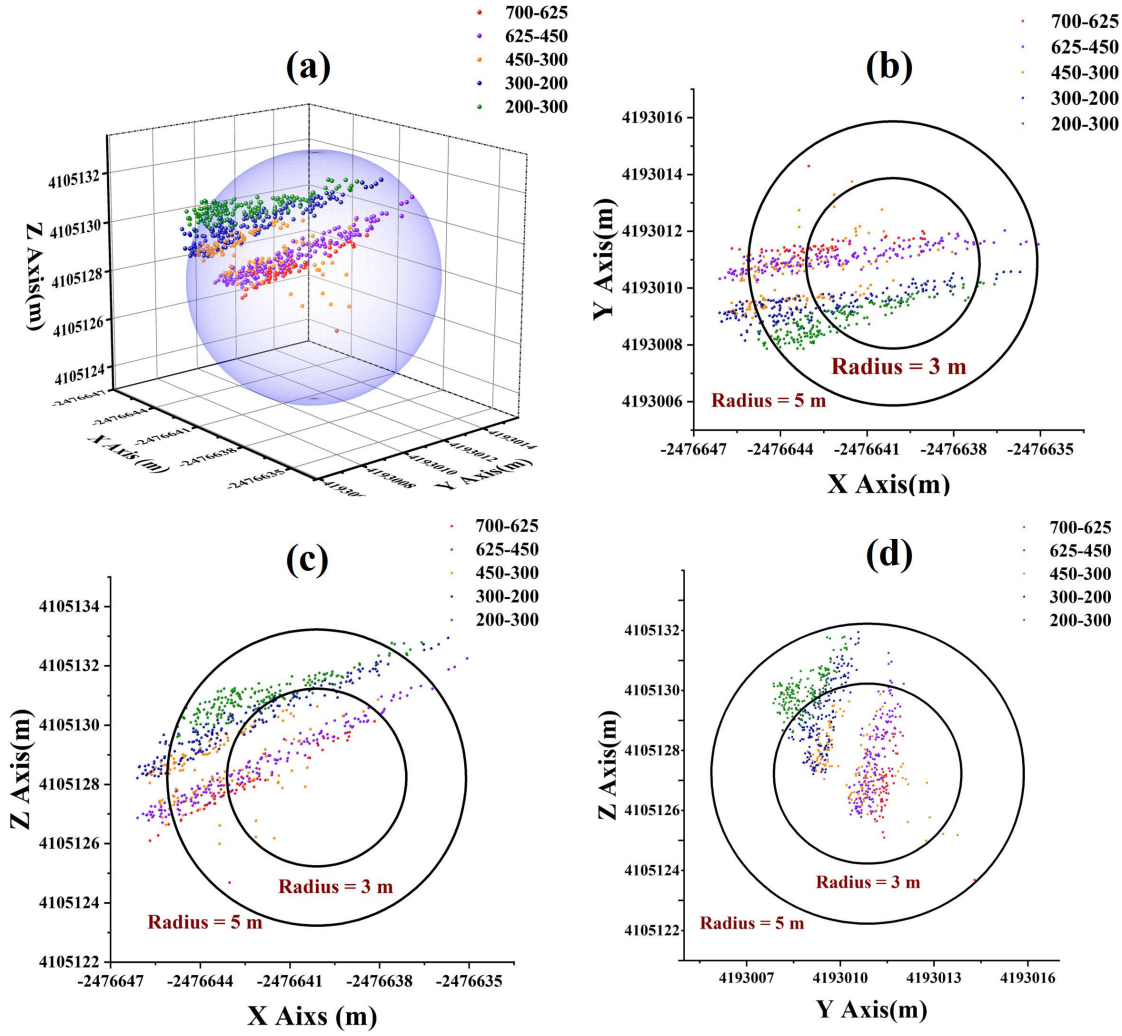

FIGURE 14. 3D coordinate map (a), XOY planes (b), XOZ planes (c), YOZ planes (d) and Offshore fall point locations.

point can be represented in Figure 14. There are two concentric circles with radii of 3m and 5m, which can clearly represent the distribution of the fall point in XOY, XOZ, and YOZ planes, and the 3D coordinate map clearly indicates the spatial location of the fall point. The magnitude of the mean square deviation indicates the degree of data discreteness. The proportion of fall point measurement errors within 5m is greater than 75%, as shown in Table 1. As the synthesis angle θ_2 of the measurement ship C2 gradually decreases, the proportion of measurement accuracy decreases. This trend is considered to be related to the calibration distortion correction parameters of the equipment. As the field of view decreases, the error increases.

The red ball indicates the position of the fall point when the cooperative target ship sails towards the fall point target from far to near, with a distance range of 700-625m. The purple ball indicates the position of the fall point at a distance of 625-500m, while the orange ball indicates the position of the fall point at a distance range of 450-300m. The blue ball represents the fall point position when the cooperative target ship is 300m away from the target and passes it until it sails away from the target by 200m. The green ball indicates the landing position when sailing away from 200-300m. The transparent purple sphere has a radius of 5m, and the measured 3D coordinates of the fall point are within a small range of 5m.

In order to avoid experimental chance, the measurement experiment was chosen to be conducted again at different times. 200 sets of data are randomly selected to test whether the accuracy range meets the demand of less than 5 m. The test results can be represented by Figure 15, where the red ball indicates the location of the randomly selected fall point, and the percentage of accuracy is 82%, which verifies the feasibility and reliability of the model.

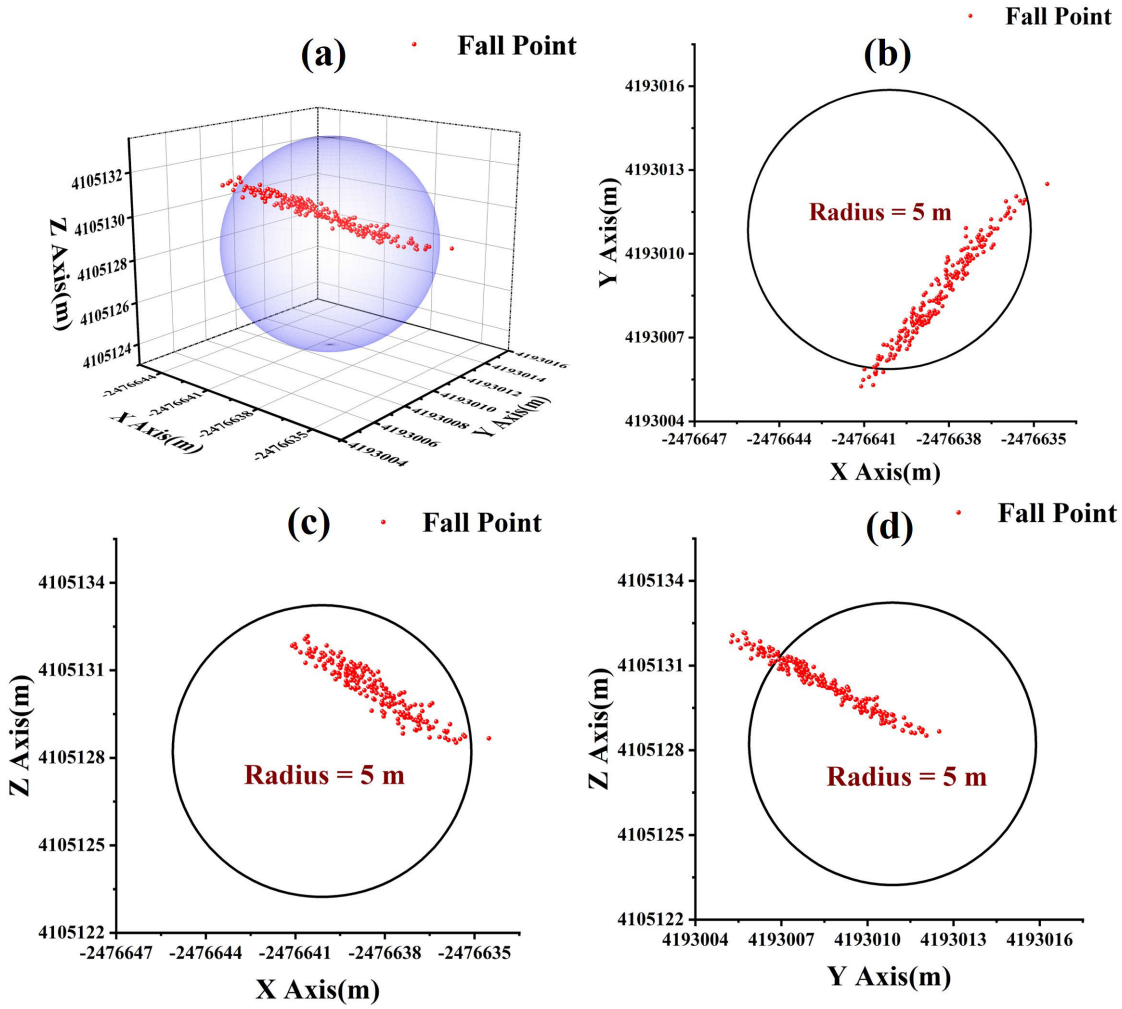

FIGURE 15. 3D coordinate map (a), XOY planes (b), XOZ planes (c), YOZ planes (d) and Sea fall point error.

V. CONCLUSION

In this paper, we have improved upon the traditional double-station intersection angle measurement of the latitude and longitude instrument and used the cone angle intersection method to process the data of the fall point at sea. The elevation information of the survey ship, the cooperative target ship, and the fall point are considered, and the influence of the radius of curvature of sea level and the height of the cooperative target ship itself is reduced. The method does not require the use of the axis angle data of the equipment, and the measurement accuracy is affected by the measurement equipment and the positioning accuracy of the cooperative target. Through multiple tests, we have fixed the sea fall point within a certain range, and the method can increase the probability of error range within 5m to more than 75%, thereby meeting the demand of measurement accuracy within 5m. The detected fall point is concentrated in a small range, which can be used to judge the hit rate of the shells. At the same time, it realizes the measurement of the fall point at a distance of up to 700m, which solves the problem of close distance in the existing photographic method of optical measurement. The method presented in this paper has instructive implications for the measurement of the fall point position of large and medium caliber naval guns.

REFERENCES

[1] B. Du, C. Pang, D. Wu, Z. Li, H. Peng, Y. Tao, E. Wu, and G. Wu, "High-speed photon-counting laser ranging for broad range of distances," *Sci. Rep.*, vol. 8, no. 1, p. 4198, Mar. 2018.

[2] B. Li, X. Sheng, A. Xia, E. Chengwen, and B. Li, "Actualize of low altitude large scale aerophotography and geodesic base on fixed-wing unmanned aerial vehicle platform," *Int. Arch. Photogramm., Remote Sens. Spatial Inf. Sci.*, vol. 37, pp. 643–646, Jan. 2011.

[3] M. Z. Lubis, W. Anurogo, S. N. Chayati, L. R. Sari, H. M. Taki, and S. Pujiyati, "Side-scan sonar investigations and marine seismic of identification object," *J. Phys., Conf.*, vol. 1442, no. 1, Jan. 2020, Art. no. 012004.

[4] P. Braca, R. Goldhahn, G. Ferri, and K. D. LePage, "Distributed information fusion in multistatic sensor networks for underwater surveillance," *IEEE Sensors J.*, vol. 16, no. 11, pp. 4003–4014, Jun. 2016.

[5] H. Liu, F. Sun, B. Fang, and X. Zhang, "Robotic room-level localization using multiple sets of sonar measurements," *IEEE Trans. Instrum. Meas.*, vol. 66, no. 1, pp. 2–13, Jan. 2017.

[6] M. N. Schmitt, "War, technology, and the law of armed conflict," *Int. Law Stud.*, vol. 82, no. 1, p. 9, 2006.
[7] M. Sadeghi, F. Behnia, and R. Amiri, "Optimal sensor placement for 2-D range-only target localization in constrained sensor geometry," *IEEE Trans. Signal Process.*, vol. 68, pp. 2316–2327, 2020.
[8] R. Amiri, S. A. R. Kazemi, F. Behnia, and A. Noroozi, "Efficient elliptic localization in the presence of antenna position uncertainties and clock parameter imperfections," *IEEE Trans. Veh. Technol.*, vol. 68, no. 10, pp. 9797–9805, Oct. 2019.
[9] M. Sadeghi, F. Behnia, R. Amiri, and A. Farina, "Target localization geometry gain in distributed MIMO radar," *IEEE Trans. Signal Process.*, vol. 69, pp. 1642–1652, 2021.
[10] M. Sadeghi, F. Behnia, and R. Amiri, "Maritime target localization from bistatic range measurements in space-based passive radar," *IEEE Trans. Instrum. Meas.*, vol. 70, pp. 1–8, 2021.
[11] W. Dong, T. Sun, J. Tian, J. Wang, Z. Song, and Q. Fu, "A target location algorithm based on millimeter wave radar," in *Proc. IEEE 6th Inf. Technol. Mechatronics Eng. Conf. (ITOEC)*, Mar. 2022, pp. 646–651.
[12] H. Ji, B. Yin, J. Zhang, and Y. Zhang, "Joint inversion of evaporation duct based on radar sea clutter and target echo using deep learning," *Electronics*, vol. 11, no. 14, p. 2157, Jul. 2022.
[13] Y. Guo, X. Wang, X. Lan, and T. Su, "Traffic target location estimation based on tensor decomposition in intelligent transportation system," *IEEE Trans. Intell. Transp. Syst.*, early access, Apr. 18, 2022, doi: 10.1109/TITS.2022.3165584.
[14] Z. Guan, L. Liu, X. Xu, A. Liu, H. Wu, J. Li, and W. Ou-Yang, "A self-powered acoustic sensor excited by ultrasonic wave for detecting and locating underwater ultrasonic sources," *Nano Energy*, vol. 104, Dec. 2022, Art. no. 107879.
[15] A. Ahmed, U. Hamid, A. Masud, M. Waqas, and S. Ali, "Simulation of ultra short baseline system for positioning of underwater vehicles," in *Proc. 19th Int. Bhurban Conf. Appl. Sci. Technol. (IBCAST)*, Aug. 2022, pp. 944–950.
[16] Y. Choi, S. Baek, C. Kim, J. Yoon, and S. M. Lee, "Simulation of AEBS applicability by changing radar detection angle," *Appl. Sci.*, vol. 11, no. 5, p. 2305, Mar. 2021.
[17] M. H. Zienkiewicz and K. Czaplewski, "Application of square M_{split} estimation in determination of vessel position in coastal shipping," *Polish Maritime Res.*, vol. 24, no. 2, pp. 3–12, Jun. 2017.
[18] K. Czaplewski, M. Waz, and M. H. Zienkiewicz, "A novel approach of using selected unconventional geodesic methods of estimation on VTS areas," *Mar. Geodesy*, vol. 42, no. 5, pp. 447–468, Sep. 2019.
[19] Y. Yang and X. Qin, "Resilient observation models for seafloor geodetic positioning," *J. Geodesy*, vol. 95, no. 7, p. 79, Jul. 2021.
[20] T. Peternel, S. Kumelj, K. Ostir, and M. Komac, "Monitoring the Potoška planina landslide (NW Slovenia) using UAV photogrammetry and tachymetric measurements," *Landslides*, vol. 14, no. 1, pp. 395–406, Feb. 2017.
[21] A. D. Kadi, E. Gokalp, and F. Kadi, "Creating orthophotos with unmanned aerial vehicles and examining its accuracy and usability in geodetic applications," *Concurrency Comput., Pract. Exper.*, vol. 34, no. 21, p. e7132, Sep. 2022. [Online]. Available: https://onlinelibrary.wiley.com/doi/abs/10.1002/cpe.7132
[22] E. J. Stich, "Geo-pointing and threat location techniques for airborne border surveillance," in *Proc. IEEE Int. Conf. Technol. for Homeland Secur. (HST)*, Nov. 2013, pp. 136–140.
[23] H. Zhang, C. Qiao, and H.-P. Kuang, "Target geo-location based on laser range finder for airborne electro-optical imaging systems," *Opt. Precis. Eng.*, vol. 27, no. 1, pp. 8–16, 2019.
[24] G.-B. Bai, Y.-M. Song, Y.-J. Zuo, X. Wang, and M.-C. Sun, "Multi-target geo-location based on airborne optoelectronic platform," *Opt. Precis. Eng.*, vol. 28, no. 10, pp. 2323–2336, 2020.
[25] Z. Feng, "Research on integrated guidance system based on data fusion of multi-sensor," in *Proc. IEEE 4th Inf. Technol., Netw., Electron. Autom. Control Conf. (ITNEC)*, Jun. 2020, pp. 2638–2643.
[26] R. Li, S. Zheng, E. Wang, J. Chen, S. Feng, D. Wang, and L. Dai, "Advances in BeiDou navigation satellite system (BDS) and satellite navigation augmentation technologies," *Satell. Navigat.*, vol. 1, no. 1, p. 12, Dec. 2020.
[27] W. Liu, J. Liu, J. Xie, and B. Jiao, "Signal-in-space range error of the global BeiDou navigation satellite system and comparison with GPS, GLONASS, Galileo, and QZSS," *J. Surveying Eng.*, vol. 149, no. 1, Feb. 2023, Art. no. 04022013.

MINGYANG LI received the B.E. degree from Yangtze University, Jingzhou, China, in 2018. He is currently pursuing the Ph.D. degree with the Changchun Institute of Optics, Fine Mechanics and Physics, Chinese Academy of Sciences, China. His main research interests include target localization and tracking, and visible and thermal infrared fusion.

YI YU is currently a Research Fellow and a Supervisor of Ph.D. candidates with the Changchun Institute of Optics, Fine Mechanics and Physics, Chinese Academy of Sciences, China. His main research interest includes optical imaging tracking and measurement.

CHENGLONG WANG received the Ph.D. degree from the Changchun University of Science and Technology, China. He is currently an Associate Research Fellow with the Changchun Institute of Optics, Fine Mechanics and Physics, Chinese Academy of Sciences, China. His main research interest includes optical imaging tracking and measurement.

TAO ZHANG received the M.S. degree from the Changchun Institute of Optics, Fine Mechanics and Physics, Chinese Academy of Sciences, China. He is currently an Associate Research Fellow with the Changchun Institute of Optics, Fine Mechanics and Physics, Chinese Academy of Sciences. His main research interests include range optical measurements and IR radiometric characterization.

XIN GUO received the M.S. degree from the Harbin Institute of Technology, Harbin, China, in 2020. She is currently an Assistant Researcher with the Changchun Institute of Optics, Fine Mechanics and Physics, Chinese Academy of Sciences, China. Her main research interest includes range data processing.

XINYU PANG received the B.E. degree from the Dalian University of Technology, Dalian, China, in 2018. He is currently pursuing the Ph.D. degree with the Changchun Institute of Optics, Fine Mechanics and Physics, Chinese Academy of Sciences, China. His main research interest includes infrared radiation characteristics measurement.